An interface element based on the partition of unity

A. Simone[1*] J. J. C. Remmers[2] G. N. Wells[1]

[1]Faculty of Civil Engineering and Geosciences, Koiter Institute Delft / Delft University of Technology
P.O. Box 5048, 2600 GA Delft, The Netherlands
[2]Faculty of Aerospace Engineering, Koiter Institute Delft / Delft University of Technology
P.O. Box 5058, 2600 GB Delft, The Netherlands

Abstract

An alternative interface finite element is developed. By using the partition of unity property of finite element shape functions, discontinuous shape functions are added to the standard finite element basis. The interface behaviour is described by extra degrees of freedom at existing nodes, avoiding the need for 'doubled nodes'. The element is kinematically equivalent to a conventional interface element but is more flexible because it allows the inclusion of interface surfaces within solid elements. In describing interface phenomena, the methodology proposed here makes possible the use of coarser meshes and it is completely insensitive to mesh topology. The new formulation is analysed throughly and comparisons are drawn with the conventional formulation.

Keywords
Interfaces, Partition of unity, Discontinuous finite elements.

*Corresponding author e-mail: a.simone@citg.tudelft.nl, Fax: +31 15 278 6383

1 INTRODUCTION

The modelling of displacement discontinuities has been based on the inclusion of interface elements at inter-element boundaries and, recently, by so-called embedded discontinuity models. In the former, a discontinuous displacement field is described through the notion of 'relative displacement' between a double set of nodes; in the latter, the discontinuity stems from the decomposition of the displacement field into a continuous and a discontinuous part. Unlike some embedded discontinuity models [1–3], interface elements are variational consistent but are limited in their applications by a dependence on mesh alignment, since it is not possible for the discontinuity surface to cross an element.

Recently, different numerical techniques have been developed which allow the use of discontinuous finite element shape functions, thus providing the natural environment for the description of interface phenomena by the inclusion of discontinuity in the displacement field [4]. The technique proposed here makes use of the partition of unity property of finite element shape functions (the sum of the shape functions must equal unity at each spatial point [5]). Within the partition of unity approach, it is possible to extend the standard approximation basis with enriched functions. This enhancement results in extra degrees of freedom for an enhanced node, without modification of the mesh topology. In this report, following Wells and Sluys [6], the standard FEM polynomial basis is enriched with discontinuous functions to model cohesive zones.

This approach generates a class of elements (PUM interface elements) which are kinematically equivalent to conventional interface elements, the key difference being the possibility of arbitrarily locating the interface within an element itself. The interface behaviour is described by an enhanced set of global degrees of freedom and by a constitutive law at the discontinuity. The formulation is general and can be used for the computational modelling of a large class of interface phenomena.

In this report, the response of PUM interface elements for one-dimensional line elements and two-dimensional quadrilateral elements is analysed and the kinematic equivalence with conventional interface elements is shown. This report is organised as follows. In the next section the kinematics and the strong and weak governing equations for a body crossed by a discontinuity are presented. The discrete equations are given in Section 3 followed by remarks on implementation aspects in Section 4. Finally, the comparison between conventional interface finite elements and partition of unity interface elements is discussed in Section 5. Details of the comparison are included in Appendix B.

2 PROBLEM FORMULATION

In this section, after reviewing the kinematics for a body crossed by a discontinuity and illustrating the link between the partition of unity method and the finite element method, the governing equations and the associated variational formulation for a body

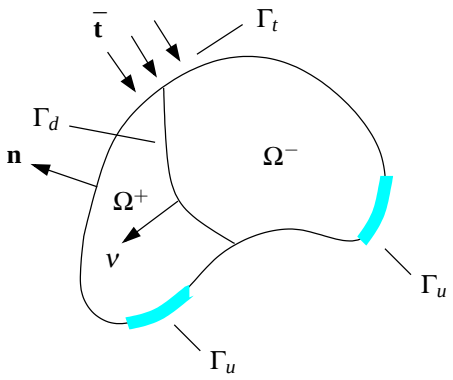

Figure 1: Body $\bar{\Omega}$ crossed by a discontinuity Γ_d.

crossed by a discontinuity are presented.

2.1 Kinematics

A body $\bar{\Omega}$ bounded by Γ and crossed by a discontinuity Γ_d is considered (Figure 1). Displacements $\bar{\mathbf{u}}$ are prescribed on Γ_u, while tractions $\bar{\mathbf{t}}$ are prescribed on Γ_t. The internal discontinuity surface Γ_d divides the body into two sub-domains, Ω^+ and Ω^- ($\Omega = \Omega^+ \cup \Omega^-$). The boundary surface of the body $\bar{\Omega}$ consists of three mutually disjoint boundary surfaces Γ_u, Γ_t and Γ_d. The displacement field can be decomposed by

$$\mathbf{u}(\mathbf{x},t) = \hat{\mathbf{u}}(\mathbf{x},t) + \mathscr{H}_{\Gamma_d}(\mathbf{x})\tilde{\mathbf{u}}(\mathbf{x},t), \tag{1}$$

where $\mathscr{H}_{\Gamma_d}(\mathbf{x})$ is the Heaviside function centred at the discontinuity surface Γ_d ($\mathscr{H}_{\Gamma_d} = 1$ if $\mathbf{x} \in \Omega^+$, $\mathscr{H}_{\Gamma_d} = 0$ if $\mathbf{x} \in \Omega^-$) and $\hat{\mathbf{u}}$ and $\tilde{\mathbf{u}}$ are continuous functions on Ω. Note that the discontinuity is introduced by the Heaviside function $\mathscr{H}_{\Gamma_d}$ at the discontinuity surface Γ_d and that the magnitude of the displacement jump $[\![\mathbf{u}]\!]$ at the discontinuity surface is given by $\tilde{\mathbf{u}}$. For small displacements, the strain field is computed as the symmetric part of the gradient of the displacement field:

$$\varepsilon = \nabla^{\mathrm{s}}\mathbf{u} = \begin{cases} \nabla^{\mathrm{s}}\hat{\mathbf{u}} & \text{if } \mathbf{x} \in \Omega^- \\ \nabla^{\mathrm{s}}\hat{\mathbf{u}} + \nabla^{\mathrm{s}}\tilde{\mathbf{u}} & \text{if } \mathbf{x} \in \Omega^+ \end{cases} \tag{2}$$

which can be written, in a compact form and away from the discontinuity ($\mathbf{x} \notin \Gamma_d$), as

$$\varepsilon = \nabla^{\mathrm{s}}\hat{\mathbf{u}} + \mathscr{H}_{\Gamma_d}\,\nabla^{\mathrm{s}}\tilde{\mathbf{u}}, \tag{3}$$

where $(\cdot)^{\mathrm{s}}$ refers to the symmetric part of $(\cdot)$.

2.2 Partitions of unity and finite elements

The construction of a partition of unity is based on the definition of *clouds* [7], which are overlapping open sets ω_i (of arbitrary shape and centred in $\mathbf{x}_i$) covering the solution domain $\bar{\Omega}$ of a boundary-value problem ($\bar{\Omega} \subset \bigcup_{i=1}^{n} \bar{\omega}_i$, where n is the number of nodes of the discretisation). A partition of unity is defined as a collection of global functions $\varphi_i(\mathbf{x})$ whose support is contained in a cloud and whose value sum to unity at each point $\mathbf{x}$ in the solution domain:

$$\sum_{i=1}^{n} \varphi_i(\mathbf{x}) = 1 \qquad \forall \mathbf{x} \in \bar{\Omega}. \tag{4}$$

Note that the partition of unit paradigm [5] is equivalent to the requirement of zeroth order consistency (rigid body modes are exactly represented).

In the finite element method, the support of a node can be understood as a cloud [8, 9] and moreover, for the global basis N_i associated to the node $\mathbf{x}_i \in \bar{\Omega}$, is

$$\sum_{i=1}^{n} N_i(\mathbf{x}) = 1 \qquad \forall \mathbf{x} \in \bar{\Omega}. \tag{5}$$

The connection between PUM and FEM is clear and FEM can be used as a framework for the construction of clouds, since also finite element shape functions satisfy the partition of unity requirement.

Using polynomial partitions of unity of order k (φ_i^k) as basis functions in a FEM framework [10], a scalar field $f(\mathbf{x})$ can be interpolated by

$$f(\mathbf{x}) = \underbrace{\sum_{i=1}^{n} \varphi_i^k(\mathbf{x}) a_i}_{\text{regular interpolation}} + \underbrace{\sum_{i=1}^{n} \varphi_i^k(\mathbf{x}) \gamma_i(\mathbf{x}) \mathbf{b}_i}_{\text{enhanced interpolation}}, \tag{6}$$

where a_i (called 'regular' degrees of freedom) are nodal values related to the basis φ_i^k and $\mathbf{b}_i = \begin{bmatrix} b_i^1 & b_i^2 & \dots & b_i^m \end{bmatrix}^{\mathrm{T}}$ (called 'enhanced' degrees of freedom) are the nodal parameters related to the basis $\gamma_i = \begin{bmatrix} \gamma_i^1 & \gamma_i^2 & \dots & \gamma_i^m \end{bmatrix}$, where m is the number of terms in the enhanced basis for node i. The terms 'regular' and 'enhanced' make reference to the fact that the 'regular' interpolation field is considered as the background field upon which the 'enhanced' interpolation field is superimposed. Note that the interpolation could have been expressed in a more compact form by including 1 in γ_i. The term corresponding to 1 is extracted and termed the regular interpolation to draw the comparison with conventional procedures. To avoid linear dependency, the order of any polynomial terms in the enhanced basis must be greater than k. Since FEM shape functions form a partition of unity, the interpolation of the scalar field $f(\mathbf{x})$ in equation (6) can be expressed as the combination of the standard finite element interpolation field and an enhanced interpolation field; the latter can be used to improve the standard interpolation. In finite element notation, the interpolation for a vector

field $\mathbf{f}(\mathbf{x})$ of a n-node enriched element with l degrees of freedom for node, with all the nodes enriched, can be written as

$$\mathbf{f}(\mathbf{x}) = \mathbf{N}(\mathbf{x})\mathbf{a} + \mathbf{N}(\mathbf{x})\mathbf{N}_\gamma(\mathbf{x})\mathbf{b}, \tag{7}$$

where $\mathbf{N}$ is a $l \times (l \times n)$ matrix containing the standard finite element shape functions, $\mathbf{N}_\gamma$ is a $(l \times n) \times (l \times m \times n)$ matrix containing the enhanced basis terms, $\mathbf{a}$ is a $(l \times n) \times 1$ vector containing standard degrees of freedom and $\mathbf{b}$ is a $(l \times m \times n) \times 1$ vector containing the enhanced degrees of freedom. The number of enhanced degrees of freedom per node ($\mathbf{b}_i$) is equal to the number of terms in the enhanced basis multiplied by the number of nodal unknowns. In standard finite elements, the matrix $\mathbf{N}_\gamma$ is empty.

As noted by Oden et al. [9], the approach of equation (7) allows the enhancement to be performed from node to node in a mesh by activating the enhanced degrees of freedom $\mathbf{b}$ when needed (a hierarchical finite element formulation based on the partition of unity method). For instance, in describing a discontinuity, if the standard displacement field is interpolated by the regular interpolation $\mathbf{Na}$, the displacement jump, described by means of a difference in displacements in conventional interface finite elements, can be described by the enhanced interpolation $\mathbf{NN}_\gamma\mathbf{b}$.

2.2.1 Discontinuities in the enhanced basis

To simulate a displacement discontinuity, the enhanced basis terms in the matrix $\mathbf{N}_\gamma$ in equation (7) are replaced by the scalar valued Heaviside function [4, 6]. This results in the $(l \times n) \times 1$ vector of enhanced degrees of freedom $\mathbf{b}$ (same dimensions as the vector of standard degrees of freedom $\mathbf{a}$) and in the $(l \times n) \times (l \times n)$ diagonal $\mathscr{H}_{\Gamma_d}\,\mathbf{H}$ matrix identifying through a 1/0 switch which degrees of freedom to enhance; $\mathbf{H}$ is the identity matrix if all the degrees of freedom of the element are enhanced.

The enhancement concerns only nodes whose support is crossed by a discontinuity. For nodes whose support is not crossed by a discontinuity, the enhanced basis is empty since the Heaviside function is a constant function over their supports and can be neglected. In the domain of an element where enhanced degrees of freedom are active, the displacement field in equation (1), expressed in a discrete format, can be written as

$$\mathbf{u} = \mathbf{Na} + \mathscr{H}_{\Gamma_d}\,\mathbf{NHb}, \tag{8}$$

in which the regular degrees of freedom $\mathbf{a}$ represent the continuum displacement field and the enhanced degrees of freedom $\mathbf{b}$ represent the displacement jump across the discontinuity Γ_d. Consequently, the strain field in equation (3), away from the discontinuity ($\mathbf{x} \notin \Gamma_d$), is equal to

$$\varepsilon = \mathbf{Ba} + \mathscr{H}_{\Gamma_d}\,\mathbf{BHb}, \tag{9}$$

where $\mathbf{B} = \mathbf{LN}$ and $\mathbf{L}$ is the differential operator

$$\mathbf{L} = \begin{bmatrix} \frac{\partial}{\partial x} & 0 & 0 \\ 0 & \frac{\partial}{\partial y} & 0 \\ 0 & 0 & \frac{\partial}{\partial z} \\ \frac{\partial}{\partial y} & \frac{\partial}{\partial x} & 0 \\ 0 & \frac{\partial}{\partial z} & \frac{\partial}{\partial y} \\ \frac{\partial}{\partial z} & 0 & \frac{\partial}{\partial x} \end{bmatrix}. \tag{10}$$

In a finite element discretisation, the resulting 'enhanced' element stiffness matrix will be assembled only for the active degrees of freedom. This allows the use of the standard operators **N**, **B** and $\mathscr{H}_{\Gamma_d}$ in place of the enhanced operators $\mathscr{H}_{\Gamma_d}$ **NH** and $\mathscr{H}_{\Gamma_d}$ **BH**, on condition that a database indicating the nodes to be enhanced exists. The extra computational cost due to the computation of the extra kinematic operators is related only to elements affected by the enhancement, which is negligible, since only relatively few elements are usually enhanced. The discretised kinematic fields are expressed by

$$\mathbf{u} = \mathbf{Na} + \mathscr{H}_{\Gamma_d}\,\mathbf{Nb} \tag{11}$$

and

$$\varepsilon = \mathbf{Ba} + \mathscr{H}_{\Gamma_d}\,\mathbf{Bb}. \tag{12}$$

2.3 Governing equations

The equilibrium equations and boundary conditions for the body $\bar{\Omega}$ (Figure 1) without body forces can be summarised by

$$\nabla\cdot\sigma = \mathbf{0} \qquad \text{in } \Omega \tag{13}$$
$$\sigma\mathbf{n} = \bar{\mathbf{t}} \qquad \text{on } \Gamma_t \tag{14}$$
$$\sigma\nu = \mathbf{t} \qquad \text{on } \Gamma_d \tag{15}$$

where σ is the Cauchy stress tensor and the last equation represents traction continuity at the the discontinuity surface Γ_d. The strong form is completed by the essential boundary condition

$$\mathbf{u} = \bar{\mathbf{u}} \qquad \text{on } \Gamma_u, \tag{16}$$

where $\bar{\mathbf{u}}$ is a prescribed displacement, and by the constitutive relation

$$\sigma = \mathbf{D}{:}\varepsilon \qquad \text{in } \Omega \tag{17}$$

for the continuum, where the constitutive fourth-order tensor $\mathbf{D}$ links the stress tensor σ to the strain tensor ε. The traction at a discontinuity is given by

$$\mathbf{t} = \mathbf{f}(\llbracket \mathbf{u} \rrbracket) \qquad \text{on } \Gamma_d, \tag{18}$$

where $\llbracket \mathbf{u} \rrbracket$ is the displacement jump across the surface Γ_d. To simplify the finite element implementation, the additional condition

$$\tilde{\mathbf{u}} = \mathbf{0} \qquad \text{on } \Gamma_u \tag{19}$$

for the magnitude of the displacement jump is imposed. The boundary condition of equation (16) now reads

$$\hat{\mathbf{u}} = \bar{\mathbf{u}} \qquad \text{on } \Gamma_u. \tag{20}$$

2.4 Variational formulation

The displacement field is discontinuous due to the presence of a discontinuity surface Γ_d and it is assumed that the displacement field is continuously differentiable away from it. The space of admissible displacements is defined by the function $\mathbf{u}(\mathbf{x},t) = \hat{\mathbf{u}}(\mathbf{x},t) + \mathscr{H}_{\Gamma_d}\,\tilde{\mathbf{u}}(\mathbf{x},t)$ with $\hat{\mathbf{u}}$ and $\tilde{\mathbf{u}} \in U$ where

$$U = \left\{ \hat{\mathbf{u}} \text{ and } \tilde{\mathbf{u}} \mid \hat{\mathbf{u}} \text{ and } \tilde{\mathbf{u}} \in H^1(\Omega) \text{ and } \hat{\mathbf{u}}_{|\Gamma_u} = \bar{\mathbf{u}},\, \tilde{\mathbf{u}}_{|\Gamma_u} = \mathbf{0} \right\} \tag{21}$$

and H^1 is the Sobolev space of first order, while the space of admissible variations is defined by the function $\mathbf{w}(\mathbf{x}) = \hat{\mathbf{w}}(\mathbf{x}) + \mathscr{H}_{\Gamma_d}\,\tilde{\mathbf{w}}(\mathbf{x})$ with $\hat{\mathbf{w}}$ and $\tilde{\mathbf{w}} \in U_0$ where

$$U_0 = \left\{ \hat{\mathbf{w}} \text{ and } \tilde{\mathbf{w}} \mid \hat{\mathbf{w}} \text{ and } \tilde{\mathbf{w}} \in H^1(\Omega) \text{ and } \hat{\mathbf{w}}_{|\Gamma_u} = \tilde{\mathbf{w}}_{|\Gamma_u} = \mathbf{0} \right\}. \tag{22}$$

To recast the strong governing equations (equations (13) to (15)) in a variational setting, the strong form is multiplied by the function $\mathbf{w}$ and then integrated over the domain Ω. The weak form results in

$$\int_\Omega \left(\hat{\mathbf{w}} + \mathscr{H}_{\Gamma_d}\,\tilde{\mathbf{w}} \right) \cdot (\nabla \cdot \sigma)\; d\Omega = 0. \tag{23}$$

The term related to the continuous part of the displacement field ($\hat{\mathbf{w}}$) can be expanded by using integration by parts, Gauss' theorem and the relationship $\sigma\mathbf{n} = \bar{\mathbf{t}}$:

$$\int_\Omega \hat{\mathbf{w}} \cdot (\nabla \cdot \sigma)\; d\Omega = \int_\Omega \nabla \cdot (\sigma \hat{\mathbf{w}})\; d\Omega - \int_\Omega \nabla^{\mathrm{s}} \hat{\mathbf{w}} : \sigma\; d\Omega = \int_{\Gamma_t} \hat{\mathbf{w}} \cdot \bar{\mathbf{t}}\; d\Gamma - \int_\Omega \nabla^{\mathrm{s}} \hat{\mathbf{w}} : \sigma\; d\Omega. \tag{24}$$

The term related to the discontinuous part of the displacement field ($\mathscr{H}_{\Gamma_d}\,\tilde{\mathbf{w}}$) is expanded using integration by parts:

$$\int_\Omega \mathscr{H}_{\Gamma_d}\,\tilde{\mathbf{w}} \cdot (\nabla \cdot \sigma)\; d\Omega = \int_{\Omega^+} \tilde{\mathbf{w}} \cdot (\nabla \cdot \sigma)\; d\Omega = \int_{\Omega^+} \nabla \cdot (\sigma \tilde{\mathbf{w}})\; d\Omega - \int_{\Omega^+} \nabla^{\mathrm{s}} \tilde{\mathbf{w}} : \sigma\; d\Omega. \tag{25}$$

Using Gauss' theorem and the traction equations $\sigma\nu = \mathbf{t}$ and $\sigma\mathbf{n} = \bar{\mathbf{t}}$, the first term of the RHS of equation (25) reads

$$\int_{\Omega^+} \nabla\cdot(\sigma\tilde{\mathbf{w}})\; d\Omega = \int_{\Gamma_t^+} \tilde{\mathbf{w}}\cdot(\sigma\mathbf{n})\; d\Gamma - \int_{\Gamma_d^+} \tilde{\mathbf{w}}\cdot(\sigma\nu)\; d\Gamma = \int_{\Gamma_t^+} \tilde{\mathbf{w}}\cdot\bar{\mathbf{t}}\, d\Gamma - \int_{\Gamma_d^+} \tilde{\mathbf{w}}\cdot\mathbf{t}\, d\Gamma, \quad (26)$$

where Γ_t^+ and Γ_d^+ are parts of the boundary $\partial\Omega^+$ of Ω^+. Using the previous relations in equation (23), the weak form reads

$$\int_{\Omega} \nabla^{\mathrm{s}}\hat{\mathbf{w}}{:}\sigma\; d\Omega + \int_{\Omega^+} \nabla^{\mathrm{s}}\tilde{\mathbf{w}}{:}\sigma\; d\Omega + \int_{\Gamma_d} \tilde{\mathbf{w}}\cdot\mathbf{t}\, d\Gamma = \int_{\Gamma_t} \left(\hat{\mathbf{w}} + \mathscr{H}_{\Gamma_d}\,\tilde{\mathbf{w}}\right)\cdot\bar{\mathbf{t}}\, d\Gamma, \quad (27)$$

in which the terms related to Γ_t and Γ_t^+ have been collected under the same integral by using the Heaviside function. Since the function $\tilde{\mathbf{w}}$ is continuous across the discontinuity and since the the notation Γ_d^+ has been introduced to indicate which part of the discontinuity is under analysis, the domain Γ_d^+ of the integral of the traction forces $\mathbf{t}$ has been changed into Γ_d.

From the decomposition of the displacement field it follows that any admissible variation $\mathbf{w}$ of $\mathbf{u}$ can be regarded as admissible variations $\hat{\mathbf{w}}$ and $\tilde{\mathbf{w}}$, thus leading to two variational statements. Taking first variation $\hat{\mathbf{w}}$ ($\tilde{\mathbf{w}} = \mathbf{0}$) and then $\tilde{\mathbf{w}}$ ($\hat{\mathbf{w}} = \mathbf{0}$), the problem is to find $\hat{\mathbf{u}}$ and $\tilde{\mathbf{u}} \in U$ such that

$$\int_{\Omega} \nabla^{\mathrm{s}}\hat{\mathbf{w}}{:}\sigma\; d\Omega = \int_{\Gamma_t} \hat{\mathbf{w}}\cdot\bar{\mathbf{t}}\, d\Gamma \quad \forall\hat{\mathbf{w}} \in U_0 \quad (28a)$$

$$\int_{\Omega^+} \nabla^{\mathrm{s}}\tilde{\mathbf{w}}{:}\sigma\; d\Omega + \int_{\Gamma_d} \tilde{\mathbf{w}}\cdot\mathbf{t}\, d\Gamma = \int_{\Gamma_t^+} \tilde{\mathbf{w}}\cdot\bar{\mathbf{t}}\, d\Gamma \quad \forall\tilde{\mathbf{w}} \in U_0. \quad (28b)$$

The second variational statement ensures that traction continuity is satisfied in a weak sense across the discontinuity Γ_d. Moreover, if the traction $\mathbf{t}$ acting on the discontinuity surface Γ_d is set to zero then the discontinuity is traction-free in a weak sense. The two variational statements in equation (28) resemble a coupled problem in which the fields $\tilde{\mathbf{u}}$ and $\hat{\mathbf{u}}$ are coupled in the continuum through the stress field and the effect of the discontinuity is taken into account by the integral over Γ_d.

3 DISCRETISATION

In this section the linearised form of the governing equations for a body crossed by a discontinuity is developed.

3.1 Kinematic description

Using a Bubnov-Galerkin approach, the kinematic fields can be discretised in each element 'affected' by the enhancement using

$$\hat{\mathbf{u}} = \mathbf{N}\mathbf{a} \qquad \tilde{\mathbf{u}} = \mathbf{N}\mathbf{b} \tag{29}$$

$$\nabla^{\mathrm{S}}\hat{\mathbf{u}} = \mathbf{B}\mathbf{a} \qquad \nabla^{\mathrm{S}}\tilde{\mathbf{u}} = \mathbf{B}\mathbf{b} \tag{30}$$

$$\hat{\mathbf{w}} = \mathbf{N}\mathbf{a}' \qquad \tilde{\mathbf{w}} = \mathbf{N}\mathbf{b}' \tag{31}$$

$$\nabla^{\mathrm{S}}\hat{\mathbf{w}} = \mathbf{B}\mathbf{a}' \qquad \nabla^{\mathrm{S}}\tilde{\mathbf{w}} = \mathbf{B}\mathbf{b}' \tag{32}$$

where the primes refer to admissible variations.

3.2 Discretised and linearised weak equations

Inserting the discrete format of the kinematic fields into equation (28), leads to two discrete weak governing equations which are valid at element level:

$$\int_{\Omega} \mathbf{B}^{\mathrm{T}}\sigma \, d\Omega = \int_{\Gamma_t} \mathbf{N}^{\mathrm{T}}\bar{\mathbf{t}} \, d\Gamma \tag{33a}$$

$$\int_{\Omega^+} \mathbf{B}^{\mathrm{T}}\sigma \, d\Omega + \int_{\Gamma_d} \mathbf{N}^{\mathrm{T}}\mathbf{t} \, d\Gamma = \int_{\Gamma_t^+} \mathbf{N}^{\mathrm{T}}\bar{\mathbf{t}} \, d\Gamma. \tag{33b}$$

From equation (33), the equivalent nodal forces related to admissible variations of $\mathbf{a}$ and $\mathbf{b}$ result in

$$\mathbf{f}_{\,\mathrm{int},a} = \int_{\Omega} \mathbf{B}^{\mathrm{T}}\sigma \, d\Gamma \tag{34a}$$

$$\mathbf{f}_{\,\mathrm{int},b} = \int_{\Omega^+} \mathbf{B}^{\mathrm{T}}\sigma \, d\Omega + \int_{\Gamma_d} \mathbf{N}^{\mathrm{T}}\mathbf{t} \, d\Gamma. \tag{34b}$$

The stress rate $\dot{\sigma}$ in the continuum is expressed in terms of nodal displacement velocities as

$$\dot{\sigma} = \mathbf{D}\dot{\varepsilon} = \mathbf{D}\left(\mathbf{B}\dot{\mathbf{a}} + \mathscr{H}_{\Gamma_d}\,\mathbf{B}\dot{\mathbf{b}}\right). \tag{35}$$

Similarly, the traction rate at a discontinuity is expressed as

$$\dot{\mathbf{t}} = \mathbf{T}[\![\dot{\mathbf{u}}]\!] = \mathbf{T}\mathbf{N}\dot{\mathbf{b}}, \tag{36}$$

where $\mathbf{T}$ relates traction rate $\dot{\mathbf{t}}$ and displacement jump rate $[\![\dot{\mathbf{u}}]\!]$. The linearised weak form is formed by inserting the above stress and traction rate expressions into the discretised weak governing equations in equation (33), thus obtaining

$$\begin{bmatrix} \mathbf{K}_{aa} & \mathbf{K}_{ab} \\ \mathbf{K}_{ba} & \mathbf{K}_{bb} \end{bmatrix} \begin{bmatrix} \Delta\mathbf{a} \\ \Delta\mathbf{b} \end{bmatrix} = \begin{bmatrix} \mathbf{f}_{\,\mathrm{ext},a,t+dt} \\ \mathbf{f}_{\,\mathrm{ext},b,t+dt} \end{bmatrix} - \begin{bmatrix} \mathbf{f}_{\,\mathrm{int},a,t} \\ \mathbf{f}_{\,\mathrm{int},b,t} \end{bmatrix}, \tag{37}$$

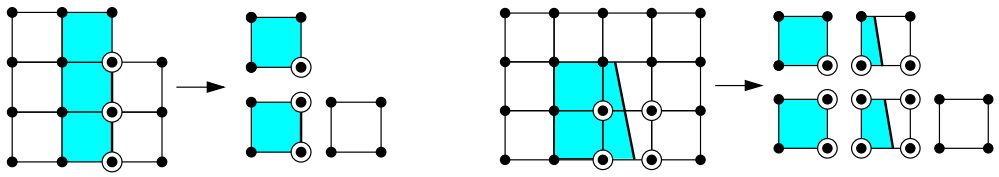

(a) (b)

Figure 2: Enhanced nodes, represented by a white circle, lying (a) on and (b) around a discontinuity. The discontinuity is represented by the heavy line and $\mathscr{H}_{\Gamma_d} = 1$ in the grey shaded zones for the enhanced elements.

where the sub-matrices are defined as

$$\mathbf{K}_{aa} = \int_{\Omega} \mathbf{B}^{\mathrm{T}}\mathbf{D}\mathbf{B}\, d\Omega \tag{38a}$$

$$\mathbf{K}_{ab} = \int_{\Omega^+} \mathbf{B}^{\mathrm{T}}\mathbf{D}\mathbf{B}\, d\Omega \tag{38b}$$

$$\mathbf{K}_{ba} = \mathbf{K}_{ab}^{\mathrm{T}} = \int_{\Omega^+} \mathbf{B}^{\mathrm{T}}\mathbf{D}\mathbf{B}\, d\Omega \tag{38c}$$

$$\mathbf{K}_{bb} = \int_{\Omega^+} \mathbf{B}^{\mathrm{T}}\mathbf{D}\mathbf{B}\, d\Omega + \int_{\Gamma_d} \mathbf{N}^{\mathrm{T}}\mathbf{T}\mathbf{N}\, d\Gamma \tag{38d}$$

and $\mathbf{f}_{\mathrm{ext}}$ are the externally applied forces (RHS of equation (33)). Note that if the material tangent matrices $\mathbf{D}$ and $\mathbf{T}$ are symmetric, symmetry of the stiffness matrix is assured.

4 ELEMENT TECHNOLOGY

The position of the discontinuity is dictated by the geometry of the problem. In situations in which the interface describes a physical boundary between two bodies, a natural choice would be to locate the discontinuity at the boundary (interface-like element, Figure 2a) to capture the strain discontinuity at the material interface. In this special case, only the nodes on the discontinuity need to be enhanced. A discontinuity can also be arbitrarily placed in the continuum (general interface-like element, Figure 2b). For an element crossed by a discontinuity, all the nodes are enhanced but the integration is carried out only in the shaded grey part of the domain (Ω_{e}^{+}) for the terms of the stiffness matrix involving the enhanced nodes. When an element has enhanced nodes and no discontinuity, the enhancement is similar to that of the interface-like element (cf. Appendix A).

The two characterisations are equivalent as they produce the same kinematic fields, the main difference regards the number of enhanced nodes. In the case of a crossing discontinuity, like in Figure 2b, the enhancement concerns a wider set of nodes. Note

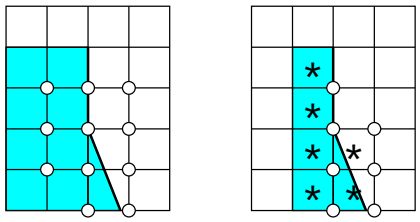

Figure 3: Procedure for the enhancement of nodes and elements: (a) all the nodes whose support is crossed by a discontinuity are enhanced and the nodes on the crack tip are constrained ; (b) only the nodes which satisfy the area criterion are kept. Enhanced nodes are indicated by the circles and enhanced elements are marked with *. The positive part of the domain is shaded grey.

that the enhancement of the kinematic fields with the Heaviside function concerns only those nodes whose support is crossed by a discontinuity and for which

$$\frac{\min\left(\Omega_{\mathrm{s}}^{+},\Omega_{\mathrm{s}}^{-}\right)}{\Omega_{\mathrm{s}}} > \text{tolerance} \tag{39}$$

where Ω_{s} is the area of the support of a node, $\Omega_{\mathrm{s}}^{+/-}$ is the area of the support of a node that belongs to $\Omega^{+/-}$, and the tolerance depends on the precision of the solver. This 'area criterion' ensures a well-conditioned global stiffness matrix in the case the discontinuity lies very close to the boundary of the support of a node and allows situations in which the discontinuity aligns with the boundary of an element to be dealt with. In the latter situation and, more generally, when the support of a node is not crossed by a discontinuity, the Heaviside function is constant and must not be added to the enhanced basis, since a constant function forms part of the span of standard polynomial shape functions, thus violating the requirements of the interpolation field of equation (6) and generating a linearly dependent system of equations. Equally important is that the displacement jump at a discontinuity tip is zero. To enforce this, discontinuity tips must coincide with element boundaries and the nodes on the boundary are not enhanced [6]. The area criterion and the requirement on the crack tip are illustrated in Figure 3 (the crack tip is in the upper part of the mesh).

Due to the presence of an integral over the discontinuity surface Γ_d, the integration scheme needs to be adjusted in order to perform the integration of the traction forces acting at a discontinuity. In the case of an interface-like element, extra integration points placed on the discontinuity suffices. It is stressed that, even if the discontinuity is placed along the boundary of two elements (see Figure 2a), the tractions at the interface-like element are integrated only along the side of the element on which the Heaviside function is equal to unity. For the general interface-like element, care must also be taken to correctly integrate the continuum contributions to the stiffness matrix on both sides of the discontinuity [4].

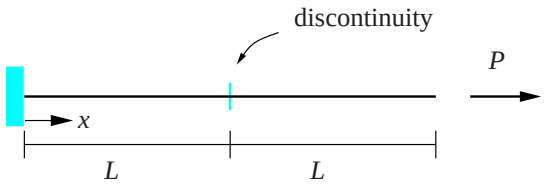

Figure 4: Geometry for the tension test (1d configuration).

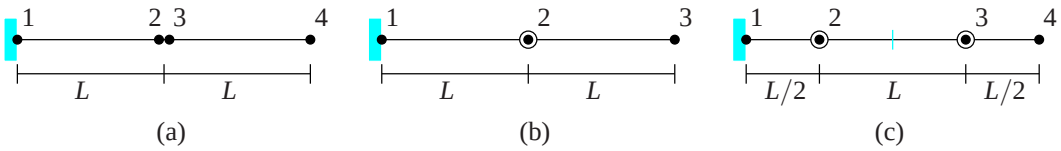

Figure 5: Discretisation for the tension test: (a) conventional interface element, (b) interface-like element and (c) and general interface-like element.

Although it is possible to activate a discontinuity after a specific condition is met, here it is assumed that the discontinuity is present from the beginning of an analysis. This keeps the implementation relatively simple and allows for a direct comparison with conventional interface elements.

5 A COMPARISON

5.1 One-dimensional tension test.

The equivalence between PUM interface elements and conventional interface elements is illustrated by means of a tension test (Figure 4). The three discretisations to be considered are depicted in Figure 5. The discontinuity Γ_d is first modelled by a conventional interface element (Figure 5a). The PUM decomposition of the displacement field is exploited for the last two discretisation (Figure 5b-c). Note that in Figure 5b the discontinuity is placed between two elements (interface-like element), while in Figure 5c it is placed within an the element (general interface-like element). The domain Ω^+ is given by $0 < x < L$. Details of the stiffness matrix computations are in Appendix A. In the following, E is the Young's modulus, A is the cross-section area and d is the stiffness of the interface/discontinuity.

5.1.1 Analysis with conventional interface element

For the bar with the discontinuity modelled by a conventional interface element (Figure 5a), assembly of local stiffness matrices into the global stiffness matrix for the

active degrees of freedom results in the system of equations

$$\begin{bmatrix} \frac{EA}{L}+d & -d & 0 \\ -d & \frac{EA}{L}+d & -\frac{EA}{L} \\ 0 & -\frac{EA}{L} & \frac{EA}{L} \end{bmatrix} \begin{bmatrix} u_2 \\ u_3 \\ u_4 \end{bmatrix} = \begin{bmatrix} 0 \\ 0 \\ P \end{bmatrix}. \tag{40}$$

Solving this system of equations yields:

$$\begin{bmatrix} u_2 \\ u_3 \\ u_4 \end{bmatrix} = \begin{bmatrix} \frac{PL}{EA} \\ \frac{P(dL+EA)}{dEA} \\ \frac{P(2dL+EA)}{dEA} \end{bmatrix}. \tag{41}$$

5.1.2 Analysis with interface-like element

Considering the discretisation with an interface-like element (Figure 5b), assembly of local stiffness matrices into the global stiffness matrix results in the global system of equations

$$\begin{bmatrix} \frac{2EA}{L} & \frac{EA}{L} & -\frac{EA}{L} \\ \frac{EA}{L} & \frac{EA}{L}+d & 0 \\ -\frac{EA}{L} & 0 & \frac{EA}{L} \end{bmatrix} \begin{bmatrix} \hat{u}_2 \\ \tilde{u}_2 \\ u_3 \end{bmatrix} = \begin{bmatrix} 0 \\ 0 \\ P \end{bmatrix}, \tag{42}$$

which after solving yields

$$\begin{bmatrix} \hat{u}_2 \\ \tilde{u}_2 \\ u_3 \end{bmatrix} = \begin{bmatrix} \frac{P(dL+EA)}{dEA} \\ -\frac{P}{d} \\ \frac{P(2dL+EA)}{dEA} \end{bmatrix}. \tag{43}$$

5.1.3 Analysis with general interface-like element

For the discretisation with the general interface-like element (Figure 5c), the global system of equations reads

$$\begin{bmatrix} \frac{3EA}{L} & -\frac{EA}{L} & \frac{5}{2}\frac{EA}{L} & -\frac{1}{2}\frac{EA}{L} & 0 \\ -\frac{EA}{L} & \frac{3EA}{L} & -\frac{1}{2}\frac{EA}{L} & \frac{1}{2}\frac{EA}{L} & -\frac{2EA}{L} \\ \frac{5}{2}\frac{EA}{L} & -\frac{1}{2}\frac{EA}{L} & \frac{5}{2}\frac{EA}{L}+\frac{d}{4} & -\frac{1}{2}\frac{EA}{L}+\frac{d}{4} & 0 \\ -\frac{1}{2}\frac{EA}{L} & \frac{1}{2}\frac{EA}{L} & -\frac{1}{2}\frac{EA}{L}+\frac{d}{4} & \frac{1}{2}\frac{EA}{L}+\frac{d}{4} & 0 \\ 0 & -\frac{2EA}{L} & 0 & 0 & \frac{2EA}{L} \end{bmatrix} \begin{bmatrix} \hat{u}_2 \\ \hat{u}_3 \\ \tilde{u}_2 \\ \tilde{u}_3 \\ u_4 \end{bmatrix} = \begin{bmatrix} 0 \\ 0 \\ 0 \\ 0 \\ P \end{bmatrix}, \tag{44}$$

discretisation	displacement in the middle section	displacement jump
conventional interface element	$u_2 = PL/EA$	$u_3 - u_2 = P/d$
interface-like element	$\hat{u}_2 + \tilde{u}_2 = PL/EA$	$\tilde{u}_2 = -P/d$
general interface-like element	$(\hat{u}_2 + \tilde{u}_2 + \hat{u}_3 + \tilde{u}_3)/2 = PL/EA$	$(\tilde{u}_2 + \tilde{u}_3)/2 = -P/d$

Table 1: Value of significant displacements for the three discretisations.

from which yields:

$$\begin{bmatrix} \hat{u}_2 \\ \hat{u}_3 \\ \tilde{u}_2 \\ \tilde{u}_3 \\ u_4 \end{bmatrix} = \begin{bmatrix} \frac{P(dL+2EA)}{2dEA} \\ \frac{P(3dL+2EA)}{2dEA} \\ -\frac{P}{d} \\ -\frac{P}{d} \\ \frac{P(2dL+EA)}{dEA} \end{bmatrix}. \tag{45}$$

The value of significant displacements is reported in table 1 (the minus sign in the displacement jump is due to the direction of the unit normal vector ν, which is pointing to Ω^+).

5.1.4 Remarks

Although this simple example gives little insight into the conceptual similarities of the two approaches (conventional interface *versus* PUM interface elements), it shows the equivalence of the results given by PUM interface elements and by conventional interface elements and highlights the differences between the two PUM interface elements. Indeed, when a discontinuity is placed at the boundary of an element, the interface-like element is very versatile since it does not require the definition of doubled nodes (like with conventional interface elements) and it is based only on one element (unlike the general interface-like element).

5.2 Two-dimensional tension test

The similarities of the two approaches (conventional interface *versus* PUM interface elements) can be analysed by means of the two-dimensional case (Figure 6) of the previous example (Poisson's ratio $= 0$). The bar is discretised by means of linear quadrilateral elements and the discontinuity is described by a conventional linear interface element and by an interface-like element. The structure of the global stiffness matrix is depicted schematically in Figure 8. When a conventional interface element is used, the displacement jump is represented by the relative displacement of doubled nodes. This

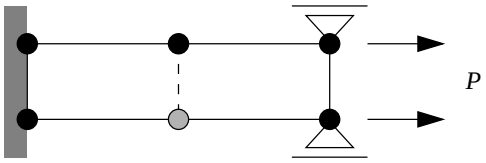

Figure 6: Geometry for the tension test (2d configuration).

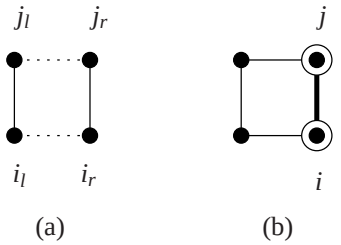

Figure 7: Sets of nodes for the description of (a) relative displacement with a conventional interface element and for (b) displacement jump with an interface-like element.

results in, for the degrees of freedom in the horizontal direction for the grey shaded node in Figure 6, the shaded rows depicted in Figure 8a. If an interface-like element is used, the displacement jump is represented by a degree of freedom and the equation to which it is related is represented by the shaded row in Figure 8b. In Figure 8, the squares represent terms related to the stiffness of the continuum while the circles are related to the stiffness of the interface/discontinuity. The white circles indicate those integrals with zero value after Newton-Cotes/Lobatto integration and are referred to as the terms representing the 'coupling' between sets of nodes. The coupling between node sets (nodes i and j in Figure 7) is here understood in the sense that, for the conventional interface element, an action on node i_r will produce not only a reaction in node i_l, but also a reaction at the j set of nodes. Similarly, for the interface-like element, an action at node i will produce a reaction at node j.

Figure 8 reveals that the interface-like element destroys the banded structure of the system for this small problem. This is a local effect related to the portion of the structure affected by the enhancement, here made more evident because of the limited number of degrees of freedom. Moreover, the terms related to the integration over the discontinuity (the circles) are concentrated in a small part of the global stiffness matrix close to the diagonal when an interface-like element is used (only one degree of freedom is necessary to describe the displacement jump). This can improve the conditioning number of the system when a high interface/discontinuity is used. Beside this, the structure of the global system is similar in both cases. The off-diagonal terms (circles in white) are acting in the same way for the two discretisations, providing the coupling between the sets of nodes related to the displacement jump.

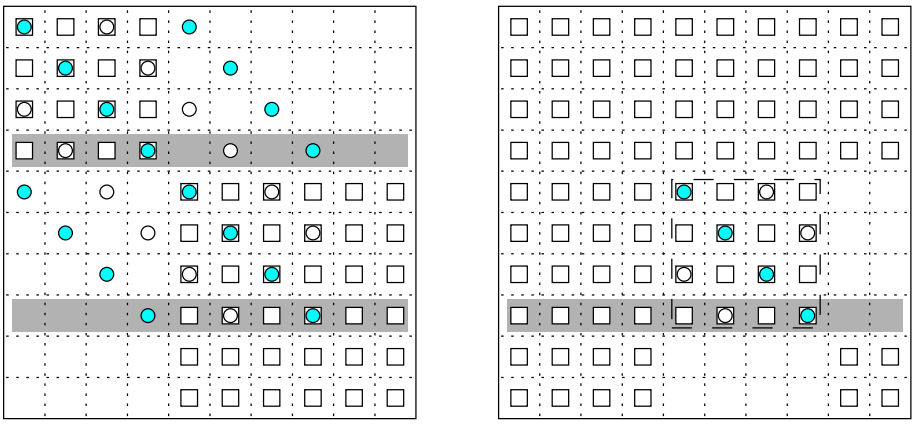

(a) (b)

Figure 8: Structure of the stiffness matrix for the discretisation with (a) conventional interface element and with (b) interface-like element.

5.3 Linear elastic analysis of a notched beam.

In Schellekens and de Borst [11], it was suggested that the aforementioned coupling is the reason for the poor performance of numerically integrated conventional interface elements, when a large traction gradient exists over an interface element. This leads to the conclusion that PUM interface elements and conventional interface elements are expected to perform similarly. To illustrate this, the two-dimensional notched beam depicted in Figure 9 has been analysed using PUM interface elements. This linear elastic test was used by Rots [12] to test the performance of numerically integrated continuous conventional interface elements. Four-node and eight-node quadrilateral elements are used under plane stress conditions. A Young's modulus of 2×10^4 N/mm^2 and a Poisson's ratio of 0.2 have been used for the continuum.

The traction-separation relation $\mathbf{t} = \mathbf{T}[\![\mathbf{u}]\!]$ of equation (36) is formulated in a local *n*,*s* coordinate system. A simple law of the type

$$\begin{bmatrix} t_n \\ t_s \end{bmatrix} = \begin{bmatrix} d_n & 0 \\ 0 & d_s \end{bmatrix} \begin{bmatrix} \tilde{u}_n \\ \tilde{u}_s \end{bmatrix} \tag{46}$$

is used, where d_n and d_s are constant, $\tilde{u}_n$ and $\tilde{u}_s$ are the displacement jumps in the local (discontinuity) reference system and t_n and t_s are the normal and tangential interface tractions. This approach is usually called the 'dummy stiffness' approach and it is used often in combination with conventional interface elements. To reproduce pure mode-I opening, only displacement jumps in the horizontal direction are activated. The notch is simulated as a traction-free discontinuity ($d_n = d_s = 0$ N/mm^3). The analyses reported by Rots show a normal traction profile along the central line of the beam which is highly dependent on the stiffness of the interface and on the chosen numerical integration scheme. In particular, it was shown that high values of the normal stiffness

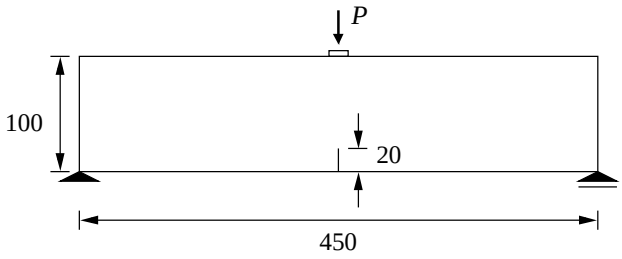

Figure 9: Notched beam. All dimensions in millimetres (depth=100 mm).

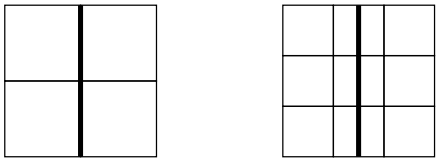

Figure 10: Schematic representation of the position of the discontinuity, represented by the heavy line, for the simulations with a structured mesh.

in combination with Gauss integration lead to significant oscillations of the normal traction profile.

The results of the analyses are reported in Figures 12 to 14, in which the normal tractions have been sampled at the integration points on the discontinuity. The stiffness d_n at the discontinuity ranges from 2×10^3 to 2×10^5 N/mm^3. Results depicted in the upper and central parts of Figures 12 and 13 and in Figure 14 have been obtained using structured meshes with the discontinuity lying on the side of the elements (element size = 5 mm, Figure 10a) or within elements (element size = 3.33 mm, Figure 10b). The mesh in Figure 11 has been used for the results depicted in the bottom parts of Figures 12 and 13. In structured meshes, PUM interface elements show the same spurious traction oscillations of conventional interface elements when a Gauss quadrature scheme is used for the integration of the traction forces at the discontinuity (upper and

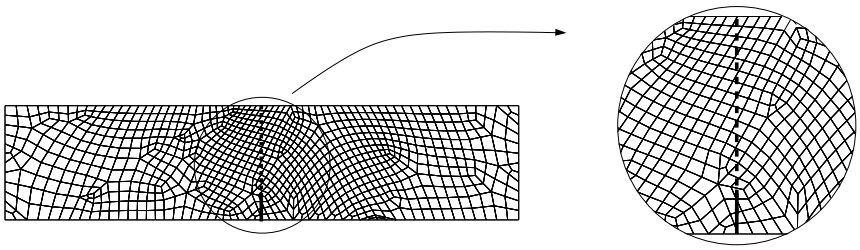

Figure 11: Notched beam with 943 elements. The discontinuity is represented by the heavy line.

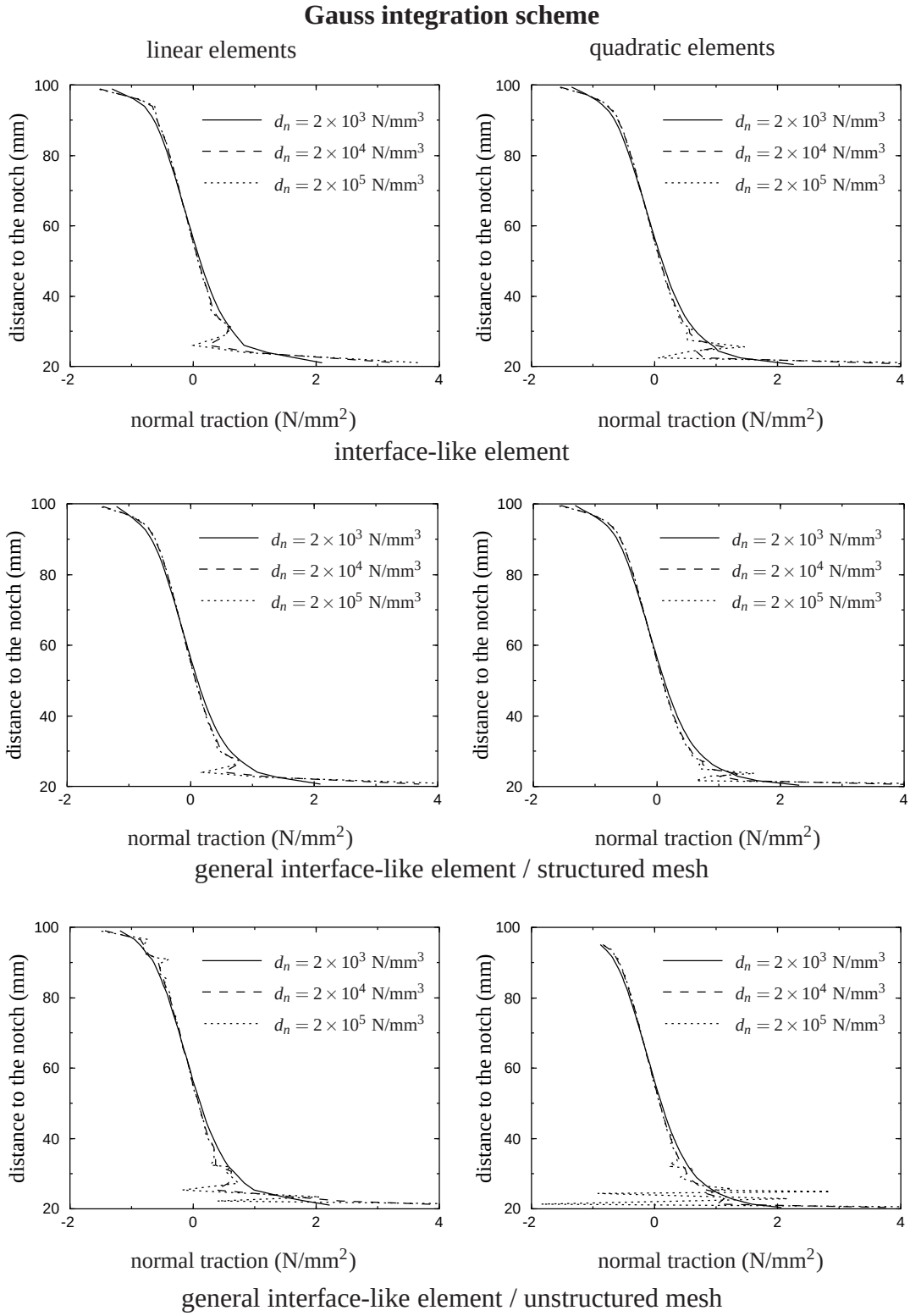

Figure 12: Traction profile in front of the notch of the beam with Gauss integration scheme for different mesh structures.

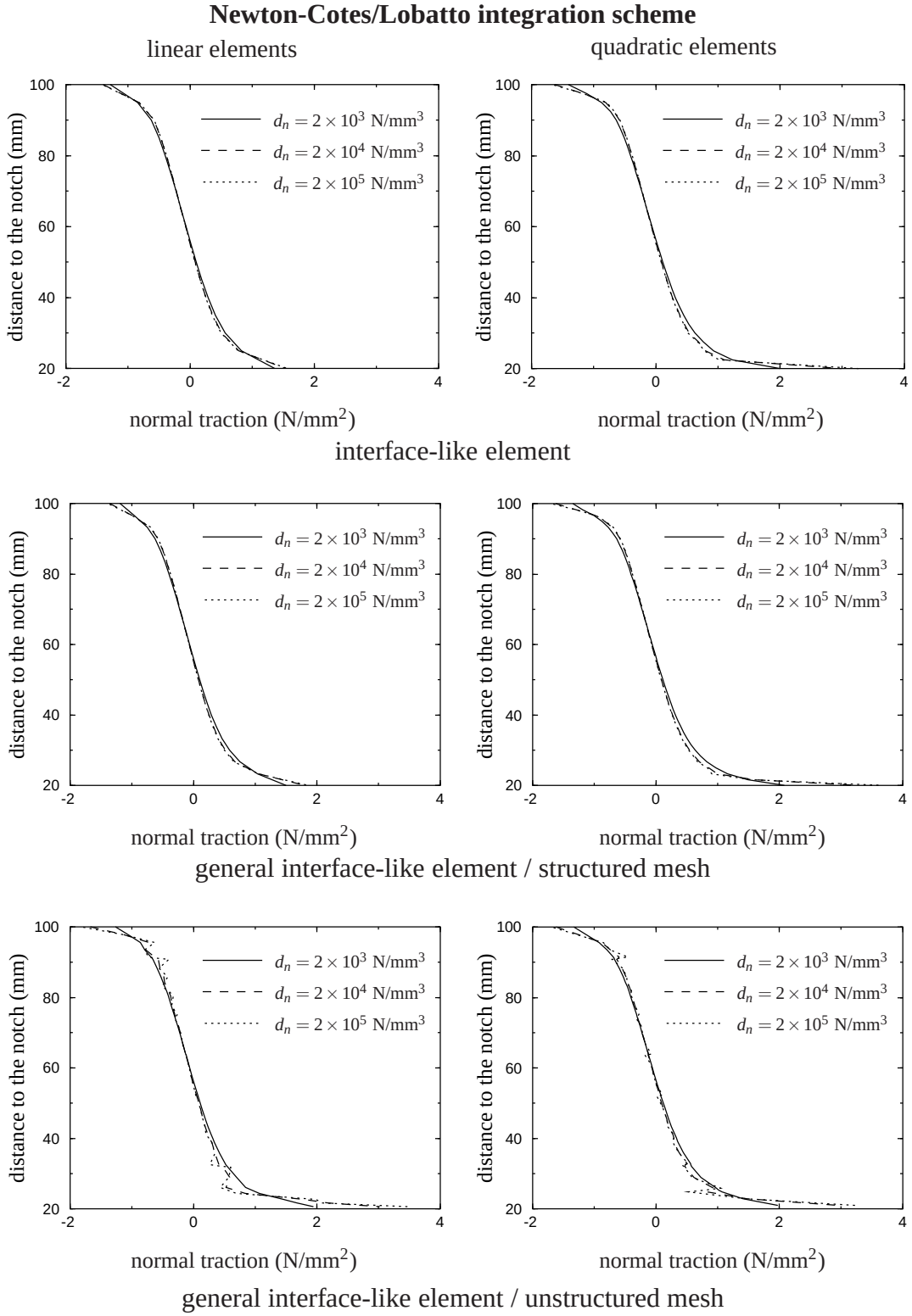

Figure 13: Traction profile in front of the notch of the beam with Newton-Cotes/Lobatto integration scheme for different mesh structures.

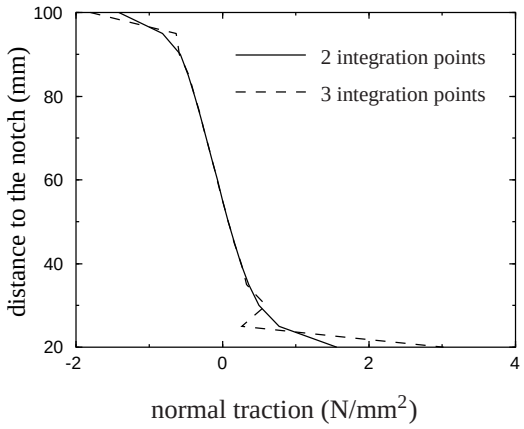

Figure 14: Effect of over-integration on the traction profile in front of the notch of the beam with linear interface-like elements and Newton-Cotes/Lobatto integration scheme ($d_n = 2 \times 10^5$ N/mm^3).

central parts of Figures 12 and 13). Only a Newton-Cotes/Lobatto integration scheme gives a smooth traction profile for all the values of the dummy stiffness. These results are similar to those reported by Schellekens and de Borst [11]. In unstructured meshes with high value of the dummy stiffness, the oscillations in the traction profile are always present (bottom parts of Figures 12 and 13). It is worthwhile to note that spurious traction oscillations are also introduced by over-integration with a Newton-Cotes/Lobatto integration scheme as reported in Figure 14 (cf. Appendix B.3).

To gain more insight into the behaviour of PUM interface elements and to draw comparisons with conventional interface elements, an eigenvalue analysis has been performed on an interface-like element. The eigenvalue analysis has been performed on the part $\int_{\Gamma_d} \mathbf{N}^{\mathrm{T}}\mathbf{T}\mathbf{N}\, d\Gamma$ of the sub-matrix $\mathbf{K}_{bb}$ which directly contributes to the stiffness of the discontinuity. Unit values for the length, the surface area and the dummy stiffnesses d_n and d_s have been assumed. The results of the eigenvalue analyses are shown in Figures 15 and 16 for an interface-like element with a discontinuity along the right vertical side. The coupling of the nodal displacements is evident when a Gauss integration scheme is used; on the contrary, the coupling disappears with a Newton-Cotes/Lobatto integration scheme. These results are very similar to those reported by Rots and Schellekens [13] and by Schellekens [14]. Consequently, with two-dimensional linear and quadratic PUM interface-like elements, only the use of a Newton-Cotes/Lobatto integration scheme for the integration of the terms related to the discontinuity Γ_d guarantees a smooth traction profile for all the values of the dummy stiffness. For general interface-like elements, this conclusion holds only under the condition that a discontinuity crosses an element from two opposite sides as depicted in the right-hand side of Figure 10. This issue is discussed in detail in Appendix B, along with the formal equivalence of PUM interface elements and conventional interface elements.

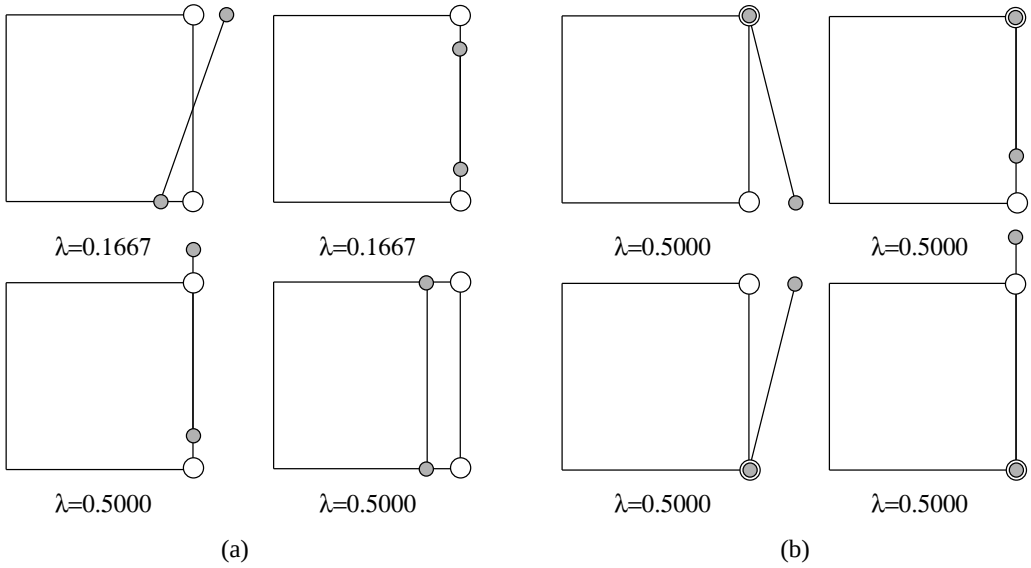

Figure 15: Eigenmodes and corresponding eigenvalues for a linear interface-like element: (a) 2–point Gauss integration; (b) 2–point Newton-Cotes/Lobatto integration.

6 CONCLUSIONS

A framework has been established for the implementation of a class of interface elements within a partition of unity method. The displacement field is enriched with the Heaviside jump function, thus providing a natural environment to describe any phenomena in which a material discontinuity is expected.

Unlike conventional interface elements, PUM interface elements do not need modification of the existing mesh to locate a discontinuity. In this approach, extra global degrees of freedom are added to the nodes that correspond to the interface. Moreover, PUM interface elements are kinematically equivalent to conventional interface elements but are more flexible because a discontinuity can arbitrarily cross the mesh. This results in a decoupling of the mesh topology and the material behaviour. In unstructured meshes however, the presence of spurious oscillations in the traction field along the discontinuity when a 'dummy stiffness' approach with high values of the dummy stiffness is used, limits the potential of the method. This can be largely avoided by activating the degrees of freedom responsible for the displacement jump when they are required, thus avoiding the initial elastic branch. But this problem may still persist if elastic unloading with high value of the elastic modulus takes place.

Acknowledgements

Financial support through the programme BEO (special fund from TU Delft for excellent research) is gratefully acknowledged (A. Simone). Financial support from the Netherlands Technology Foundation (STW) is gratefully acknowledged (G. N. Wells).

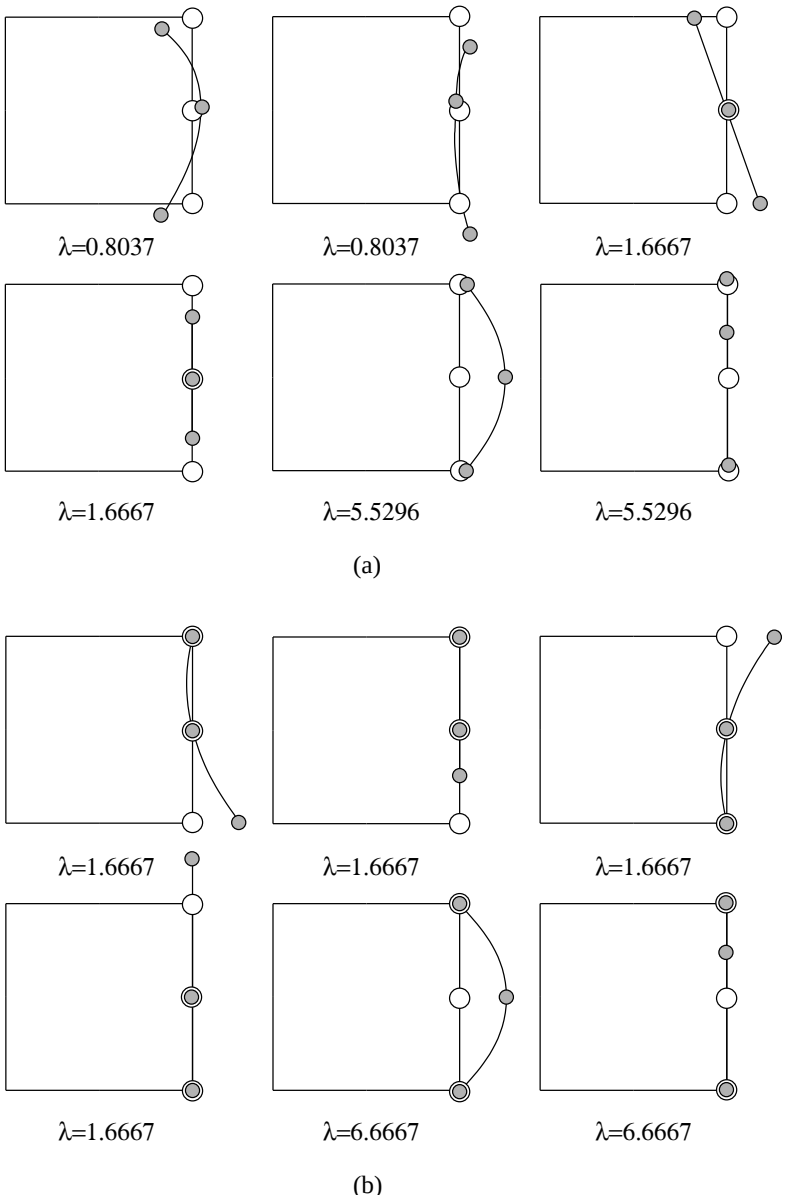

Figure 16: Eigenmodes and corresponding eigenvalues for a quadratic interface-like element: (a) 3–point Gauss integration; (b) 3–point Newton-Cotes/Lobatto integration.

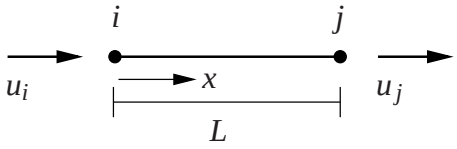

Figure A1: One-dimensional truss element.

A STIFFNESS MATRIX COMPUTATION FOR PUM INTERFACE ELEMENTS

In the following, the computation of the stiffness matrices for truss elements are performed. The degrees of freedom for an enhanced element have been ordered in the sequence $\left[\begin{array}{cccc} \tilde{u}_i & \hat{u}_i & \tilde{u}_j & \hat{u}_j \end{array}\right]$. The notation $\mathbf{B}_{\mathscr{H}} = \mathbf{BH}$ has been used (cf. Section 2.2.1). This results in the following expressions for the sub-matrices in equation (38):

$$\mathbf{K}_{aa} = \int_{\Omega} \mathbf{B}^{\mathrm{T}}\mathbf{D}\mathbf{B}\, d\Omega \tag{A1a}$$

$$\mathbf{K}_{ab} = \int_{\Omega^+} \mathbf{B}^{\mathrm{T}}\mathbf{D}\mathbf{B}_{\mathscr{H}}\, d\Omega \tag{A1b}$$

$$\mathbf{K}_{ba} = \mathbf{K}_{ab}^{\mathrm{T}} = \int_{\Omega^+} \mathbf{B}_{\mathscr{H}}^{\mathrm{T}}\mathbf{D}\mathbf{B}\, d\Omega \tag{A1c}$$

$$\mathbf{K}_{bb} = \int_{\Omega^+} \mathbf{B}_{\mathscr{H}}^{\mathrm{T}}\mathbf{D}\mathbf{B}_{\mathscr{H}}\, d\Omega + \int_{\Gamma_d} \mathbf{N}^{\mathrm{T}}\mathbf{T}\mathbf{N}\, d\Gamma. \tag{A1d}$$

in which the effect of the Heaviside jump function has been considered by the integration over Ω^+.

A.1 Truss and conventional interface element

For completeness, the stiffness matrices of the truss and the conventional interface elements are reported. For a one-dimensional truss element (Figure A1)

$$\mathbf{K}_{\text{truss}} = \frac{EA}{L}\left[\begin{array}{cc} 1 & -1 \\ -1 & 1 \end{array}\right], \tag{A2}$$

where E is the Young's modulus and A is the cross-section area. A one-dimensional conventional interface element can be understood as a translational spring element (Figure A2) with stiffness d for which

$$\mathbf{K}_{\text{int}} = d\left[\begin{array}{cc} 1 & -1 \\ -1 & 1 \end{array}\right]. \tag{A3}$$

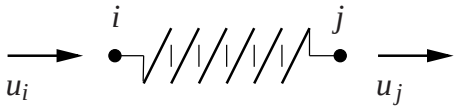

Figure A2: One-dimensional conventional interface (spring) element.

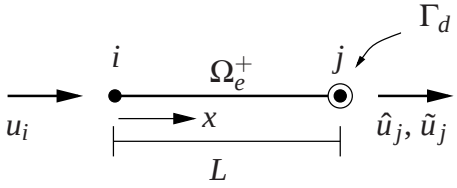

Figure A3: Interface-like truss element.

A.2 Interface-like truss element

The sub-matrices in equation (A1) are expanded for an interface-like truss element. In the element depicted in Figure A3, the discontinuity is placed at the right-hand end. Sub-matrix $\mathbf{K}_{aa}$ is the same as $\mathbf{K}_{\text{truss}}$. Only the node placed on the discontinuity (node j) is enhanced and thus $\mathbf{B}_{\mathscr{H}} = \mathbf{BH} = \frac{1}{L}[0\ 1]$ with

$$\mathbf{H} = \begin{bmatrix} 0 & 0 \\ 0 & 1 \end{bmatrix}. \tag{A4}$$

The integrals with the subscript $\mathscr{H}$ can be expanded as

$$\mathbf{K}_{ab} = \int_{\Omega^+} \mathbf{B}^{\mathrm{T}}\mathbf{D}\mathbf{B}_{\mathscr{H}}\, d\Omega = \int_0^L \mathbf{B}^{\mathrm{T}}\mathbf{D}\mathbf{B}_{\mathscr{H}}\, d\,x = \frac{EA}{L}\begin{bmatrix} 0 & -1 \\ 0 & 1 \end{bmatrix} \tag{A5}$$

and

$$\mathbf{K}_{ba} = \int_{\Omega^+} \mathbf{B}_{\mathscr{H}}^{\mathrm{T}}\mathbf{D}\mathbf{B}\, d\Omega = \int_0^L \mathbf{B}_{\mathscr{H}}^{\mathrm{T}}\mathbf{D}\mathbf{B}\, d\,x = \frac{EA}{L}\begin{bmatrix} 0 & 0 \\ -1 & 1 \end{bmatrix}. \tag{A6}$$

For $\mathbf{K}_{bb}$, the volume integral reads

$$\int_{\Omega^+} \mathbf{B}_{\mathscr{H}}^{\mathrm{T}}\mathbf{D}\mathbf{B}_{\mathscr{H}}\, d\Omega = \int_0^L \mathbf{B}_{\mathscr{H}}^{\mathrm{T}}\mathbf{D}\mathbf{B}_{\mathscr{H}}\, d\,x = \frac{EA}{L}\begin{bmatrix} 0 & 0 \\ 0 & 1 \end{bmatrix} \tag{A7}$$

and the surface integral is evaluated on $x = L$ to obtain

$$\int_{\Gamma_d} \mathbf{N}^{\mathrm{T}}\mathbf{T}\mathbf{N}\, d\Omega = \left(\mathbf{N}^{\mathrm{T}}\mathbf{T}\mathbf{N}\right)\,|_{x=L} = d\begin{bmatrix} 0 & 0 \\ 0 & 1 \end{bmatrix}. \tag{A8}$$

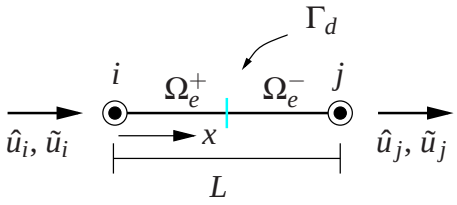

Figure A4: Embedded-discontinuity truss element.

Assembly of the sub-matrices into the element stiffness matrix gives

$$\mathbf{K}_{pum} = \begin{bmatrix} \frac{EA}{L} & -\frac{EA}{L} & 0 & -\frac{EA}{L} \\ -\frac{EA}{L} & \frac{EA}{L} & 0 & \frac{EA}{L} \\ 0 & 0 & 0 & 0 \\ -\frac{EA}{L} & \frac{EA}{L} & 0 & \frac{EA}{L}+d \end{bmatrix} \tag{A9}$$

and, after deleting the third row and column for the unused third degree of freedom,

$$\mathbf{K}_{pum} = \begin{bmatrix} \frac{EA}{L} & -\frac{EA}{L} & -\frac{EA}{L} \\ -\frac{EA}{L} & \frac{EA}{L} & \frac{EA}{L} \\ -\frac{EA}{L} & \frac{EA}{L} & \frac{EA}{L}+d \end{bmatrix}. \tag{A10}$$

A.3 General interface-like truss element

Discontinuity crossing the element. The sub-matrices in equation (A1) are expanded for a truss element with a discontinuity in the middle section (Figure A4). Sub-matrix $\mathbf{K}_{aa}$ is the same as $\mathbf{K}_{\text{truss}}$. The nodes are both enhanced ($\mathbf{B}_{\mathscr{H}} = \mathbf{B}$) and $\mathscr{H}_{\Gamma_d} = 1$ for $x < L/2$. The integrals are expanded as

$$\mathbf{K}_{ab} = \int_{\Omega^+} \mathbf{B}^{\mathrm{T}}\mathbf{D}\mathbf{B}_{\mathscr{H}}\, d\Omega = \int_0^{L/2} \mathbf{B}^{\mathrm{T}}\mathbf{D}\mathbf{B}\, d\,x = \frac{EA}{2L}\begin{bmatrix} 1 & -1 \\ -1 & 1 \end{bmatrix} \tag{A11}$$

$$\mathbf{K}_{ba} = \int_{\Omega^+} \mathbf{B}_{\mathscr{H}}^{\mathrm{T}}\mathbf{D}\mathbf{B}\, d\Omega = \int_0^{L/2} \mathbf{B}^{\mathrm{T}}\mathbf{D}\mathbf{B}\, d\,x = \frac{EA}{2L}\begin{bmatrix} 1 & -1 \\ -1 & 1 \end{bmatrix}. \tag{A12}$$

For $\mathbf{K}_{bb}$, the volume integral reads

$$\int_{\Omega^+} \mathbf{B}_{\mathscr{H}}^{\mathrm{T}}\mathbf{D}\mathbf{B}_{\mathscr{H}}\, d\Omega = \int_0^{L/2} \mathbf{B}^{\mathrm{T}}\mathbf{D}\mathbf{B}\, d\,x = \frac{EA}{2L}\begin{bmatrix} 1 & -1 \\ -1 & 1 \end{bmatrix} \tag{A13}$$

and the surface integral is evaluated on $x = L/2$ to obtain

$$\int_{\Gamma_d} \mathbf{N}^{\mathrm{T}}\mathbf{T}\mathbf{N}\, d\Omega = \left(\mathbf{N}^{\mathrm{T}}\mathbf{T}\mathbf{N}\right)\,|_{x=L/2} = \frac{d}{4}\begin{bmatrix} 1 & 1 \\ 1 & 1 \end{bmatrix}. \tag{A14}$$

Assembly of the sub-matrices into the element stiffness matrix gives

$$\mathbf{K}_{pum} = \begin{bmatrix} \frac{EA}{L} & -\frac{EA}{L} & \frac{EA}{2L} & -\frac{EA}{2L} \\ -\frac{EA}{L} & \frac{EA}{L} & -\frac{EA}{2L} & \frac{EA}{2L} \\ \frac{EA}{2L} & -\frac{EA}{2L} & \frac{EA}{2L}+\frac{d}{4} & \frac{EA}{2L}+\frac{d}{4} \\ -\frac{EA}{2L} & \frac{EA}{2L} & \frac{EA}{2L}+\frac{d}{4} & \frac{EA}{2L}+\frac{d}{4} \end{bmatrix}. \tag{A15}$$

Discontinuity not crossing the element. In this special case, there is only one node to enhance and there is no discontinuity. The element is considered as an interface-like element in which no discontinuity is considered. The stiffness matrix results in

$$\mathbf{K}_{pum} = \frac{EA}{L} \begin{bmatrix} 1 & -1 & -1 \\ -1 & 1 & 1 \\ -1 & 1 & 1 \end{bmatrix}. \tag{A16}$$

B THE FORMAL EQUIVALENCE OF PUM INTERFACE ELEMENT AND CONVENTIONAL INTERFACE ELEMENT

The equivalence of the two approaches (PUM interface element and conventional interface element) is demonstrated for line interface elements and two-dimensional interface-like elements. The general case of a crossing discontinuity is also analysed. The key point in drawing the comparison is that the two approaches use the same constitutive model at the interface, with the only difference being the way in which the displacement jump is described. Conventional interface elements use the relative displacement of doubled nodes while in PUM interface elements the displacement jump is naturally introduced in the formulation as a degree of freedom. The similarities of the two approaches will be highlighted by the analysis of the matrices related to the behaviour of the interface.

B.1 Conventional continuous interface element

The stiffness matrix of a conventional m-node line interface element [12] is

$$\mathbf{K} = b \int_{\xi=-1}^{\xi=+1} \mathbf{B}^{\mathrm{T}} \mathbf{C} \mathbf{B} \frac{\partial x}{\partial \xi} \, d\xi, \tag{B1}$$

where b is the thickness of the interface, $\mathbf{B}$ is a $2 \times 2m$ matrix containing shape functions N_i:

$$\mathbf{B} = \begin{bmatrix} -\mathbf{N} & \mathbf{N} & \mathbf{0} & \mathbf{0} \\ \mathbf{0} & \mathbf{0} & -\mathbf{N} & \mathbf{N} \end{bmatrix} \tag{B2}$$

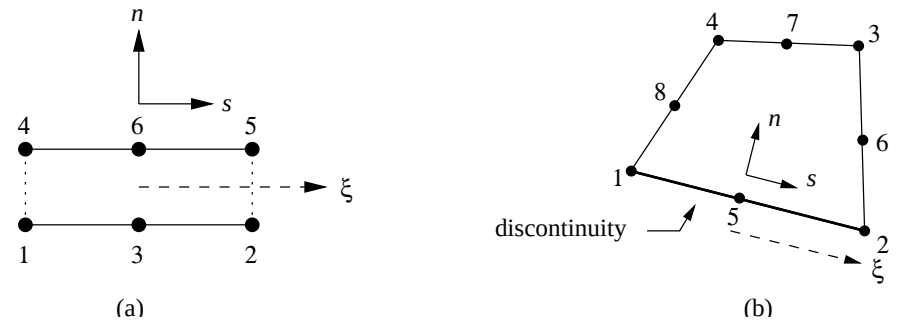

Figure B1: Quadratic field interface modelling with (a) 6-node line interface element and (b) 8-node interface-like element.

with

$$\mathbf{N} = \left[\; N_1, ..., N_m \; \right] \tag{B3}$$

and ξ is a normalised coordinate. The interface constitutive matrix $\mathbf{T}$ relating tractions and relative displacements has the same structure as $\mathbf{T}$ in equation (46). The degrees of freedom have been ordered in the sequence $\left[\; {u_n}^1, ..., {u_n}^m \quad {u_s}^1, ..., {u_s}^m \; \right]$ according to the node numbering of Figure B1a. For conventional linear line interface element the $\mathbf{N}$ matrix is equal to

$$\mathbf{N} = \left[\; \tfrac{1}{2}(1-\xi) \quad \tfrac{1}{2}(1+\xi) \; \right] \tag{B4}$$

while for conventional quadratic line interface elements it reads

$$\mathbf{N} = \left[\; \tfrac{1}{2}\left(-\xi+\xi^2\right) \quad \tfrac{1}{2}\left(\xi+\xi^2\right) \quad \left(1-\xi^2\right) \; \right]. \tag{B5}$$

Expansion of the term $\mathbf{B}^{\mathrm{T}}\mathbf{C}\mathbf{B}$ results in a block diagonal matrix:

$$\mathbf{B}^{\mathrm{T}}\mathbf{C}\mathbf{B} = \begin{bmatrix} \mathbf{K}_n & \mathbf{0} \\ \mathbf{0} & \mathbf{K}_s \end{bmatrix}, \tag{B6}$$

where $\mathbf{K}_i$ is given by

$$\mathbf{K}_i = d_i \begin{bmatrix} \bar{\mathbf{K}} & -\bar{\mathbf{K}} \\ -\bar{\mathbf{K}} & \bar{\mathbf{K}} \end{bmatrix}. \tag{B7}$$

where d_i is the stiffness at the interface in the direction i. The structure of the sub-matrix $\bar{\mathbf{K}}$ depends on the interpolation along the conventional interface element. For line elements it results in

$$\bar{\mathbf{K}} = \begin{bmatrix} N_1^2 & N_1 N_2 \\ N_1 N_2 & N_2^2 \end{bmatrix}. \tag{B8}$$

Analytical integration (and a 2–point Gauss integration scheme) of the terms $N_i N_j$ in equation (B8) results in

$$\bar{\mathbf{K}} = \frac{1}{3}\begin{bmatrix} 2 & 1 \\ 1 & 2 \end{bmatrix}; \tag{B9}$$

a 2–node Newton-Cotes/Lobatto integration scheme gives

$$\bar{\mathbf{K}} = \begin{bmatrix} 1 & 0 \\ 0 & 1 \end{bmatrix}. \tag{B10}$$

For a conventional quadratic line interface element is

$$\bar{\mathbf{K}} = \begin{bmatrix} N_1^2 & N_1N_2 & N_1N_3 \\ N_2N_1 & N_2^2 & N_2N_3 \\ N_3N_1 & N_3N_2 & N_3^2 \end{bmatrix}. \tag{B11}$$

Analytical integration (and a 2–point Gauss integration scheme) results in

$$\bar{\mathbf{K}} = \frac{1}{15}\begin{bmatrix} 4 & -1 & 2 \\ -1 & 4 & 2 \\ 2 & 2 & 16 \end{bmatrix} \tag{B12}$$

while a 3–node Newton-Cotes/Lobatto integration scheme gives

$$\bar{\mathbf{K}} = \frac{1}{3}\begin{bmatrix} 1 & 0 & 0 \\ 0 & 1 & 0 \\ 0 & 0 & 4 \end{bmatrix}. \tag{B13}$$

B.2 Interface-like element

For a generic plane interface-like element with m nodes on the side of the discontinuity, the contribution of $\mathbf{K}_{bb}$ on Γ_d is

$$\mathbf{K}_{bb,\Gamma_d} = \int_{\Gamma_d} \mathbf{N}^{\mathrm{T}}\mathbf{T}\mathbf{N}\, d\Gamma = b\int_{\xi=-1}^{\xi=+1} \mathbf{N}^{\mathrm{T}}\mathbf{T}\mathbf{N}\frac{\partial x}{\partial \xi}\, d\xi, \tag{B14}$$

in which $\mathbf{N}$ reduces to a $2\times 2m$ matrix containing the shape functions related to the side on which the discontinuity lies (side $\overline{12}$ in Figure B1b):

$$\mathbf{N} = \begin{bmatrix} \bar{\mathbf{N}} & \mathbf{0} \\ \mathbf{0} & \bar{\mathbf{N}} \end{bmatrix} \tag{B15}$$

with

$$\bar{\mathbf{N}} = \begin{bmatrix} N_1, ..., N_m \end{bmatrix}. \tag{B16}$$

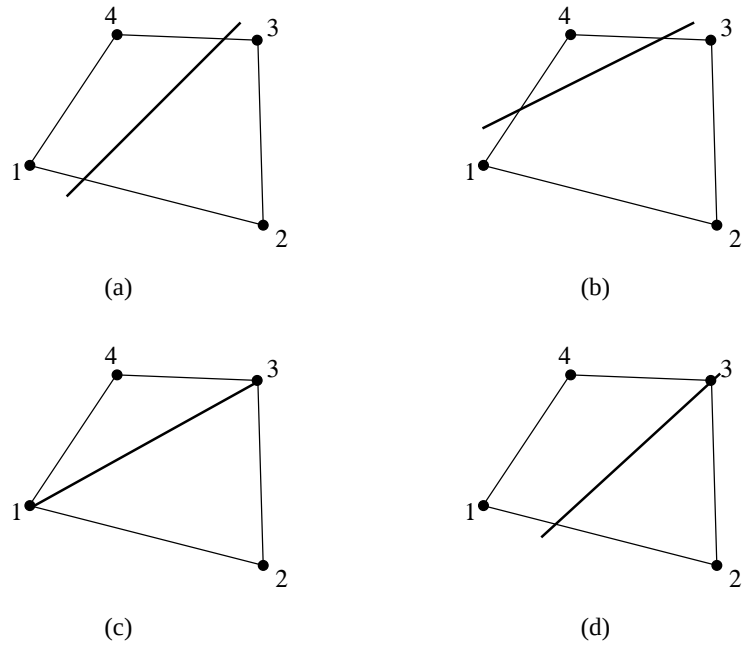

Figure B2: Possible configurations for a discontinuity crossing a general interface-like quadrilateral element.

The sequence $\left[\begin{array}{cccc} u_x{}^1, \ldots, u_x{}^m & u_y{}^1, \ldots, u_y{}^m \end{array} \right]$, according to the node numbering of Figure B1b, has been used for the ordering of the degrees of freedom in equation (B15). Expansion of $\mathbf{K}_{bb,\Gamma_d}$ gives

$$\mathbf{K}_{bb,\Gamma_d} = \left[\begin{array}{cc} \bar{\mathbf{K}}_n & \mathbf{0} \\ \mathbf{0} & \bar{\mathbf{K}}_s \end{array} \right], \tag{B17}$$

where $\bar{\mathbf{K}}_i = d_i \bar{\mathbf{K}}$, d_i is the stiffness at the discontinuity surface in the direction i and $\bar{\mathbf{K}}$ has the structure of $\mathbf{K}$ given previously for conventional line interface elements.

It is therefore demonstrated that conventional line interface elements and PUM interface-like elements have the same stiffness matrix and the same block diagonal structure for the terms related to the discontinuity. It is also worthwhile noting that the coupling appears if over-integration is used in the numerical integration of $\mathbf{K}_{bb,\Gamma_d}$ with a Newton-Cotes/Lobatto integration scheme (see Figure 14).

B.3 General interface-like element

When a discontinuity crosses an element (general interface-like element of Figure B2), all the nodes of the element are enhanced and the vector $\bar{\mathbf{N}}$ of equation (B16) contains all the shape functions of the element. In the following, only the linear quadrilateral

element is analysed. For this element the matrix $\bar{\mathbf{K}}$ is given by

$$\bar{\mathbf{K}} = \begin{bmatrix} N_1^2 & N_1N_2 & N_1N_3 & N_1N_4 \\ N_2N_1 & N_2^2 & N_2N_3 & N_2N_4 \\ N_3N_1 & N_3N_2 & N_3^2 & N_3N_4 \\ N_4N_1 & N_4N_2 & N_4N_3 & N_4^2 \end{bmatrix}. \tag{B18}$$

In the case of Figure B2a, the use of a 2–point Newton-Cotes/Lobatto integration scheme will delete the coupling between the nodes lying on side $\overline{12}$ and $\overline{34}$; more specifically, the terms N_1N_3, N_1N_4, N_2N_3 and N_2N_4 cancel. When a discontinuity is placed such as the one in Figure B2b, the coupling is to be understood between node 4 and the remaining nodes. By using a 2–point Newton-Cotes/Lobatto integration scheme, the coupling is only partially reduced (see bottom part of Figures 12 and 13) but it is still present since the term N_3N_4 does not cancel. The limit cases of Figures B2c,d fall under the the same category of Figure B2a. Analogous considerations hold for quadratic quadrilateral elements. The case of a linear or quadratic triangular element with crossing discontinuity is analogous to that of Figure B2b and the presence of spurious oscillations with Gauss or Newton-Cotes/Lobatto integration scheme has been confirmed by van Zail (private communication, 2001).

References

[1] Oliver J. Modelling strong discontinuities in solid mechanics via strain softening constitutive equations. Part 2: Numerical simulation. *International Journal for Numerical Methods in Engineering* 1996; **39**(21):3601–3623.

[2] Armero F, Garikipati K. An analysis of strong discontinuities in multiplicative finite strain plasticity and their relation with the numerical simulation of strain localization. *International Journal of Solids and Structures* 1996; **33**(20–22):2863–2885.

[3] Wells GN. *Discontinuous Modelling of Strain Localisation and Failure*. Ph.D. thesis, Delft University of Technology 2001.

[4] Moës N, Dolbow J, Belytschko T. A finite element method for crack growth without remeshing. *International Journal for Numerical Methods in Engineering* 1999; **46**(1):131–150.

[5] Melenk JM, Babuška I. The partition of unity finite element method: Basic theory and applications. *Computer Methods in Applied Mechanics and Engineering* 1996; **139**(1–4):289–314.

[6] Wells GN, Sluys LJ. A new method for modelling cohesive cracks using finite elements. *International Journal for Numerical Methods in Engineering* 2001; **50**(12):2667–2682.

[7] Duarte CAM, Oden JT. *Hp* clouds – An *hp* meshless method. *Numerical Methods for Partial Differential Equations* 1996; **12**(6):673–705.

[8] Oden JT, Duarte CA. Clouds, cracks and FEM's. In *Recent Developments in Computational and Applied Mechanics*, BD Reddy, ed. International Center for Numerical Methods in Engineering, CIMNE, Barcelona, Spain 1997; 302–321.

[9] Oden JT, Duarte CA, Zienkiewicz OC. A new cloud-based *hp* finite element method. *Computer Methods in Applied Mechanics and Engineering* 1998; **153**(1–2):117–126.

[10] Taylor RL, Zienkiewicz OC, Oñate E. A hierarchical finite element method based on the partition of unity. *Computer Methods in Applied Mechanics and Engineering* 1998; **152**(1–2):73–84.

[11] Schellekens JCJ, de Borst R. On the numerical integration of interface elements. *International Journal for Numerical Methods in Engineering* 1993; **36**:43–66.

[12] Rots JG. *Computational Modeling of Concrete Fracture*. Ph.D. thesis, Delft University of Technology 1988.

[13] Rots JG, Schellekens JCJ. Interface elements in concrete mechanics. In *Computer Aided Analysis and Design of Concrete Structures*, N Bićanić, HA Mang, eds. Pinerigde Press, Swansea, U.K. 1990; 909–918.

[14] Schellekens JCJ. Interface elements in finite element analysis. Technical Report 25.2-90-5-17, Delft University of Technology, Delft, the Netherlands 1990.